Did ice streams shape the largest channels on Mars?

Edwin S. Kite[1,2] and Richard C. A. Hindmarsh[3]

Received 29 April 2007; revised 7 July 2007; accepted 10 August 2007; published 3 October 2007.

[1] The largest channels on Mars are the Northwestern Slope Valleys (NSVs) of Tharsis, which have previously been interpreted as the probable erosional trace of catastrophic flooding. It is argued here that ice-streaming within ancient ice sheets emplaced by atmospheric precipitation at high mean obliquity may instead account for these channels, explaining similarities between the region and terrestrial Pleistocene subglacial landscapes. An ice-sheet model shows extensive basal melting in and only in the NSV region, and ice streams which have significant erosive power. **Citation:** Kite, E. S., and R. C. A. Hindmarsh (2007), Did ice streams shape the largest channels on Mars?, *Geophys. Res. Lett.*, *34*, L19202, doi:10.1029/2007GL030530.

1. Introduction

[2] The Northwestern Slope Valleys (NSVs), west of the Tharsis volcanic rise on Mars, have been described as probable catastrophic flood channels [*Dohm et al.*, 2000]. Because they dwarf the water-carved circum-Chryse channels in depth, width and estimated discharge, the flood-channel hypothesis has major implications for the hydrology of Tharsis [*Dohm et al.*, 2001], and entails a filling timescale of order weeks for the smooth northern plains, which may have played host to an ocean in the past. However, sourcing and sustaining the required peak discharges is problematic, warranting consideration of alternative hypotheses such as ice action or wind. Here we test the ice hypothesis; our work does not exclude a role for wind action, previously proposed to have shaped the ridges and valleys of this region [*Ward*, 1979].

[3] The NSVs lie between the largest, eastern lobes of finely-layered deposits termed the Medusae Fossae Formation (MFF), which straddle the equator. These deposits mantle the hemispheric dichotomy boundary scarp (Figure 1a) which divides southern cratered uplands from smooth northern plains, and the lobes of the MFF rise above the level of the southern highlands. The enigmatic MFF materials have been interpreted as tuffs [*Hynek et al.*, 2003], ignimbrites [*Scott and Tanaka*, 1982], platform carbonates [*Parker*, 1991], loess, windblown dust [*Tanaka*, 2000], ice sheet deposits [*Schultz and Lutz*, 1988], or some combination. The Amazonian or perhaps latest Hesperian MFF lobes, and underlying materials, are bounded by the NSVs.

[4] Mars' obliquity varies with periodicity 125 kyr and amplitude generally $<5°$ about a mean (φ, $25°$ since 5 Mya). φ is subject to steplike chaotic transitions, most recently from $35°$ to $25° \sim 5$ Mya, and almost certainly exceeded $45°$ once or more during the last 4 Gyr [*Laskar et al.*, 2004]. General Circulation Models (GCMs) indicate equatorward migration of water at $\varphi \geq 40°$ [*Mischna et al.*, 2003], precipitating to form an equatorial ice necklace. Orographic precipitation from ice clouds on the western flank of Tharsis would be expected to seed a large ice sheet, and the formation of ice deposits on Tharsis seems a robust result from all GCMs [*Mischna and Richardson*, 2006].

[5] Landforms resembling retreat moraines suggest cold-based Late Amazonian mountain glaciers on the NW flanks of some of the volcanoes that crown the Tharsis massif [*Scott and Zimbelman*, 1995; *Forget et al.*, 2006]. Ice sheet modelling is being used to help synthesize these observations [*Shean et al.*, 2007].

[6] As an alternative to the catastrophic-flood hypothesis for the NSVs, and in view of the increasingly strong evidence for high-obliquity ice ages, we use terrestrial analogues and an ice-sheet model to make the case for partly warm-based, much more voluminous ice sheets in earlier (latest Noachian – Early Amazonian) times, extending down the western flank of the Tharsis rise into the NSVs, discharging into Amazonis Planitia and limning Olympus Mons. The ice-sheets we model were of volume were of volume more than three times greater than that of Mars' present day polar caps, and possibly well over half the size of the Laurentide ice-sheet at the Last Glacial Maximum (LGM).

2. Comparison With Terrestrial Palaeo-Ice-Sheet Landscapes

[7] High-quality orbitally-acquired topography is now available for Earth at latitudes between 56 S and 60 N (from C-band interferometric synthetic aperture radar [*Rabus et al.*, 2003]) and Mars (from laser altimetry [*Smith et al.*, 2001]), allowing analogous landscapes to be compared in some detail. Shuttle Radar Topography Mission data shows that certain Pleistocene subglacial landscapes on Earth, such as the Straits of Magellan region, Argentina/Chile [*Rabassa and Clapperton*, 1990], and Manitoba Escarpment, Canada [*Fenton et al.*, 1994], resemble the NSV region at 10–1000 km scales (Figure 1).

[8] Both terrestrial and martian landscapes have very wide, straight, smooth-floored, steep sided, subparallel troughs with sharp margins, separated by lenticular or teardrop-plan lobes, which are elevated above surrounding terrain. The lobes and troughs are oriented parallel to regionally steep long-baseline tilts, which slope away from planetary topographic highs. The Martian lobes have 2–3 times greater relief, and are also situated on a 2–3 times steeper long-baseline tilt. Ice-sheet reconstructions for the Early Pleistocene show the Bahía Inútil and Magellan Strait

[1]Department of Earth Sciences, Cambridge University, Cambridge, UK.
[2]Now at Department of Earth and Planetary Science, University of California, Berkeley, California, USA.
[3]Physical Science Division, British Antarctic Survey, Natural Environment Research Council, Cambridge, UK.

0094-8276/07/2007GL030530$05.00

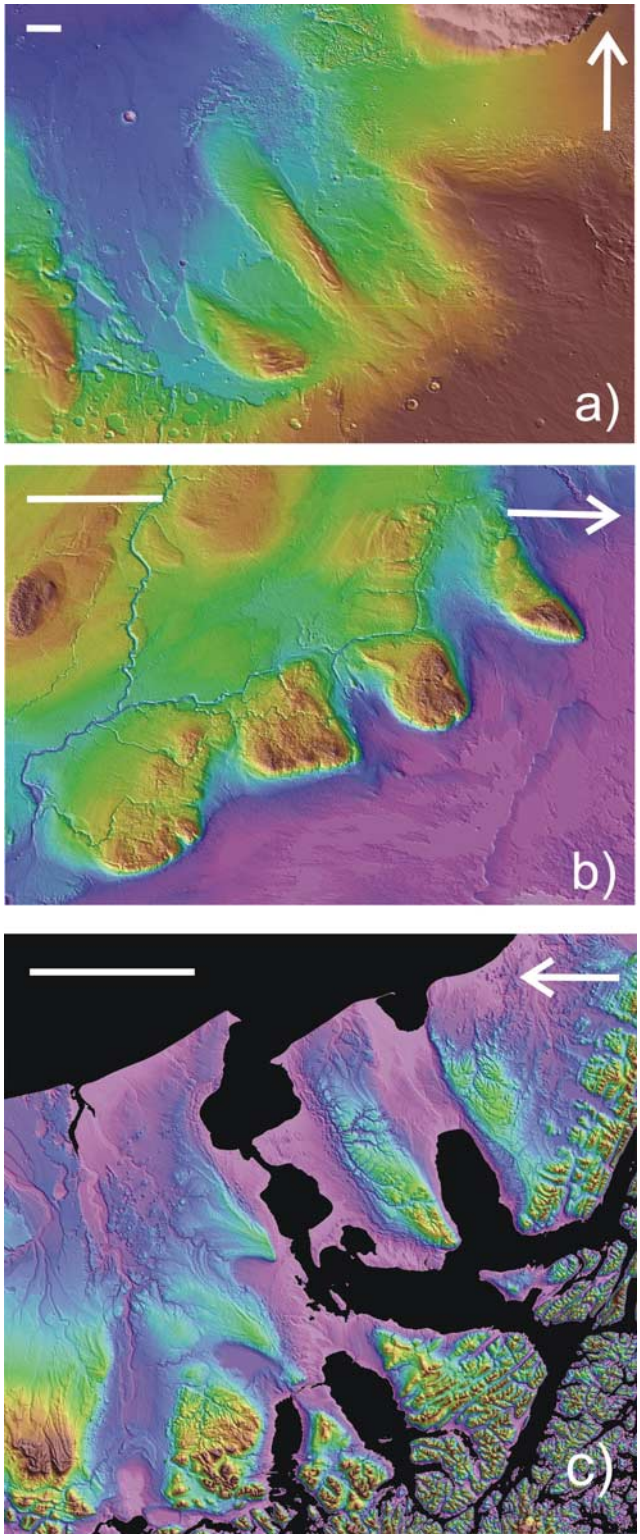

Figure 1. Terrestrial and Martian landscapes of selective linear erosion. Colour elevation draped over shaded relief; colour scale saturates at high elevations. Arrows point north. Scale bars are 100 km long. Inferred primary ice flow direction is from bottom to top in each case. (a) Northwestern Slope Valleys, Mars. Maximum lobe relief 2100 m. (b) Manitoba Escarpment, Canada, Earth. Maximum lobe relief 500 m. (c) Straits of Magellan, Argentina/Chile, Earth. Maximum lobe relief 600 m.

lobes of the Patagonian Ice Sheet extending near the edge of the continental shelf, streamlining their channels down to the present coastline [*Rabassa et al.*, 2000]. On the Manitoba Escarpment, the Laurentide ice sheets amplified pre-existing topography by widening river valleys, creating broad troughs, and preferentially depositing drift on pre-existing highs. Detailed isopach maps of the Western Canada Sedimentary Basin [*Fenton et al.*, 1994] show that till thickness is 200–300 m on the lobes, and <50 m in the troughs. These data show that ice-sheet processes more than doubled pre-Quaternary relief on the Manitoba Escarpment. Field mapping suggests that the troughs and lobes of the Straits of Magellan region and Manitoba Escarpment were defined by fast-flowing ice at or near the pressure melting point. These features can appear whether ice is incising into soft or hard material. If morphologically similar landforms are assumed to be formed in essentially the same manner on different planetary surfaces, this would suggest palaeo-ice streaming in the NSVs. If this hypothesis is correct, an ice sheet model with boundary conditions appropriate for high-obliquity Mars should yield ice streams in and only in the NSVs.

3. Model Description and Inputs

[9] We use a thermo-mechanically coupled ice-sheet model [*Hindmarsh*, 2001] with shallow ice approximation mechanics on a grid with size $\frac{1}{2}^\circ \times \frac{1}{2}^\circ$ at the equator. The domain is sufficiently large that the ice-sheet never reaches the boundary. Inputs are basal topography, mean annual accumulation/ablation rate, surface temperature and areothermal heat flux.

[10] Net annual water-ice precipitation is derived from the last 3 simulated years of output from the Geophysical Fluid Dynamics Laboratory Mars GCM ($\varphi = 45^\circ$, resolution $5^\circ \times 6^\circ$ [*Mischna et al.*, 2003]), interpolated to ice-sheet model resolution. The zonal distribution of ice is sensitive to the settling rate of water ice particles [*Mischna and Richardson*, 2006]. An intermediate rate is used, yielding a zonal distribution dominated by orographic precipitation on the W flank of Tharsis and with a maximum accumulation rate of ~50 mm/a (Figure 2a), in good agreement with the Laboratoire de Météorologie Dynamique model [*Forget et al.*, 2006].

[11] The pattern of accumulation is held constant during ice sheet growth. This is an oversimplification for terrestrial ice-sheets as increasing land surface elevation (through ice sheet growth) disfavours precipitation on land versus the ocean. Mars lacks oceans, and ice is unstable at high latitudes when $\varphi \geq 40^\circ$. Consequently, total accumulation rate is determined by loss of water from a high- or mid-latitude reservoir; this water must precipitate near the equator. More detailed meteorological processes will undoubtedly affect the exact distribution of accumulation on the ice-sheet, but for the present modelling this is a detail.

[12] The role of the planetary regolith as a store for ice and conduit for water vapor is neglected. The regolith sink saturates on Myr timescales, leaving the surface as the only long-term sink for water ice [*Mischna*, 2004]. A permeable Tharsis regolith could allow ice sheet recharge of the circum-Chryse flood channels [*Harrison and Grimm*, 2004].

[13] The annual ablation rate outside the accumulation zone is set to be constant, but this approximation is

permissible for our purposes as computed ice-stream location is fairly insensitive to variations in ablation rate (compare Figures 2b and 2e). Surface temperature is parameterized by an annually-averaged temperature at datum elevation (218 K or 228 K) that brackets GCM output, and a mean lower atmosphere lapse rate of -2.5 K km^{-1}, the value measured by the Viking Orbiters [*Zurek et al.*, 1992].

[14] Lithospheric heat flux, Q, is varied between 22 mW.m^{-2}, appropriate for present-day Mars, and 66 mW.m^{-2}; gravity/topography admittance confines heat flows >40 mW.m^{-2} to the Noachian [*McGovern et al.*, 2004]. Two end-member responses of the lithosphere to ice load are modelled. In one case, the lithosphere is rigid, while in the other, the lithosphere flexes under the ice load with an elastic thickness $D = k\Delta T/Q$, where k is lithospheric thermal conductivity (2.5 W.K^{-1}.km^{-1}), and ΔT is the difference between surface temperature and the plastic failure temperature of the lithospheric material (assumed constant, 700 K [*McKenzie et al.*, 2005]). The time constant of subsidence is very uncertain for Mars, so we model endmember, rapid subsidence (with time constant 3 kyr [*Le Meur and Huybrechts*, 1996]). This time constant is partly determined by the size of the terrestrial ice-sheets to which it applies; our ice-sheet turns out to be of comparable breadth to Quaternary terrestrial ice-sheets. Orbiting radar shows negligible flexural subsidence beneath the present day polar caps [*Plaut et al.*, 2007].

[15] Additional ice-stream motion due to sliding lubricated by basal melt is not explicitly modelled, because flow velocities depend on unknown past bed conditions. Rapid sliding creates additional heating which increases basal melting, so ignoring sliding is a conservative assumption if one seeks to demonstrate the existence of ice streams. The initial conditions are ice-free, and the ice-sheet models are run for 1 Myr, bringing the ice sheet close to equilibrium.

4. Model Results

[16] In keeping with the accumulation distribution prescribed by the GCM, the initial accumulation area is principally on the western flank of Tharsis, with a smaller accumulation area on the eastern flank. As the ice builds up, the margin expands into the ablation zone. Initially the basal temperature $\theta_{(b)}$ is well below the pressure-melting point, and ice viscosity is consequently high, with little flow apart from down the flanks of Olympus Mons. As ice accumulates on and between the Tharsis Montes and Olympus Mons, the basal temperature increases through insulation by the thickening overlying ice and frictional heating, the viscosity in the basal ice decreases, and NW-trending downslope flow moves the ice into the ablation zone through the NSVs. The ice thickens sufficiently to overtop the inter-trough lobes. East of the Tharsis Montes, flow

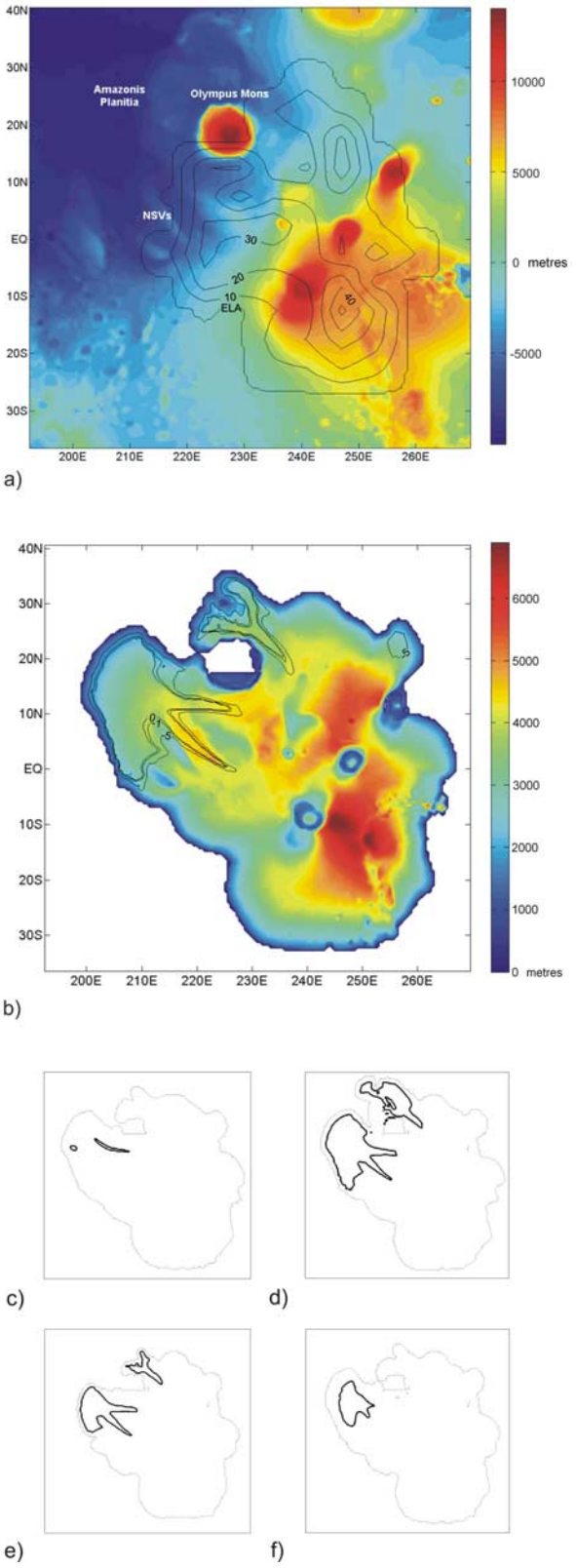

Figure 2. (a) Model input. Topography draped over shaded relief. Colour scale is elevation in m. Black contours give net ice accumulation rate in mm/a with interval 10 mm/a, lowest is zero. (b) Model output. Black contours are isotherms at 5 K, 1 K, and 0 K below the pressure-melting point. Colour scale gives ice sheet thickness in m. Parameters are Q = 33 mW.m^{-2}, uniform 33 mm/a ablation, rigid lithosphere. (c, d, e, f) Model output. Solid line demarcates area of basal melting, dotted line is ice sheet margin. Inputs as in Figure 2b, but with: Figure 2c, Q = 22 mW/m^{-2}; Figure 2d, flexing lithosphere; Figure 2e, uniform 66 mm/a ablation and flexing lithosphere; and Figure 2f, accumulation and ablation rates reduced by a factor of 4.

velocities are very small, and ice does not extend far beyond the accumulation zone. For the models discussed here, steady state mean ice sheet thickness is in the range 3–4.5 km, and the breadth is $\sim 3 \times 10^3$ km. Adjusting the melting-point for pressure-dependency makes little difference to the results. For the case $Q = 22$ mW.m^{-2} with a rigid lithosphere (typical of present day heat flow estimates), basal melting only occurs in small patches >200 km from the edge of the ice sheet (Figure 2c). With $Q = 33$ mW.m^{-2} (appropriate for the Early Amazonian or Late Hesperian) basal melting occurs in all of the Northwestern Slope Valleys, which are tributary to a $\sim 9 \times 10^5$ km^2 warm-based ice lobe extending north. A much smaller ($\sim 1 \times 10^5$ km^2) warm-based region is predicted north of Olympus Mons (Figure 2b).

[17] When $Q = 44$ mW.m^2, corresponding to the Noachian or perhaps to more recent convective overturn episodes [*Scott and Wilson*, 2003], the equilibrium ice sheet has very widespread basal melting, with wet-based ice encircling Olympus Mons. Note that present-day topography may not be a good approximation to the Noachian topography of West Tharsis, even at the coarse scale of the GCM grid. Ice sheet volumes at equilibrium range from $2.5–5.4 \times 10^7$ km^3, and basal melting does not begin in the NSV region until $1–2 \times 10^7$ km^3 ice has accumulated. Allowing flexure has similar effects to increasing surface temperature by the product of lapse rate and the mean subsidence. In both cases, the warmer ice-sheet surface leads to more extensive basal melting. Whereas an enhanced greenhouse effect (i.e., a 10 K surface temperature increase) reduces ice volume by 10%, allowing flexure has little effect on steady ice volume. With flexure permitted at $Q = 22$ mW.m^{-2}, the contiguous area of basal melting in the NSVs is 6×10^5 km^2, rising to $>1 \times 10^6$ km^2 at $Q = 33$ mW.m^{-2} (Figure 2d).

[18] In the terrestrial analogue landsystems, fast-flowing ice has greatly enhanced pre-Pleistocene topography, by broadening river valleys and preferentially depositing till on lobe tops. To test for the importance of this topographic enhancement, the MFF was backstripped by detrending NSV topography and truncating the lobes near their bases. Basal melting is still confined to the troughs.

5. Discussion and Conclusions

[19] If GCMs are a good guide to the ancient distribution of ice on Mars, the requirement for basal melting to have taken place during the final episode of ice stream activity in the NSVs constrains lithospheric heat flux and volatile inventory at that time. A low heat flux requires a sufficient amount of planetary surface volatiles to provide the ice thicknesses necessary for basal melting. The model shows that streaming in a H_2O ice sheet requires $>10^7$ km^3 ice to be transferred to the equatorial region. This lower limit might be reduced by adding additional factors to the ice-sheet model, such as a firn layer with low thermal conductivity (raising $\theta_{(b)}$), sliding (leading to faster computed discharges), or formation of methane clathrate [*McMenamin and McGill*, 2006] (lowering the melting point, inducing streaming). The combined volume of the polar layered deposits on Mars today is $\sim 3 \times 10^6$ km^3, probably insufficient to allow streaming in equatorial ice-sheets during high-obliquity episodes during the present epoch. In contrast, during the Hesperian, freezing and sublimation over $10^5–10^6$ a [*Kreslavsky and Head*, 2002] of $\sim 2.3 \times 10^7$ km^3 water debouched into the northern plains from the circum-Chryse channels [*Carr and Head*, 2003] could have readily sourced the required ice volumes.

[20] The formation of dusty lag deposits in the high-latitude water source region is not considered. We have assumed that polar ice sublimes rapidly at high obliquity, and delivery of water ice to the equatorial regions is limited only by the vapour transport capacity of the atmosphere. If an impermeable lag deposit acts as an effective diffusion barrier, vapour transport is instead limited by aeolian deflation and impact exhumation of sub-lag ice [*Mischna and Richardson*, 2005]. Better understanding of vapour diffusion through lag [e.g. *Hudson et al.*, 2007] would allow this constraint to be relaxed. As a sensitivity test, the accumulation and ablation rates were reduced by factors of 2 and 4 (with correspondingly longer model integration periods). The slower ice flow rates out of the accumulation zone lower the shear heating, and the area of basal melt in the NSVs is reduced but not eliminated (Figure 2f).

[21] MFF photogeology is dominated by evidence of aeolian deflation, and inner scarps within the westernmost NSV indicate modification by floodwaters, probably sourced from Mangala Valles. Because the upper MFF significantly postdates NSV formation, this result is compatible with the ice-stream hypothesis.

[22] The ice stream hypothesis can be tested further. If a thick ice carapace overlay the study region for a substantial fraction of its history, the size-frequency distribution of craters would be modified, with small craters underrepresented. Detailed geological mapping [*Zimbelman*, 2006] should reveal periglacial and glacial landforms and landsystems. Smaller MFF lobes W of the NSV region host esker networks (e.g. THEMIS frame V0587001), indicating basal melting. If the MFF lobes have volatile-rich cores [*Head and Kreslavsky*, 2001], these may be detected by the 15–25 MHz SHAllow RADar (SHARAD) aboard the Mars Reconnaissance Orbiter. A growing ice sheet alters local topography, albedo and thermal inertia. Although the computational expense of coupling an ice sheet model to a GCM is prohibitive, a climate model of intermediate complexity should be used to explore the feedbacks between ice accumulation and climate at high obliquity.

[23] Since West Tharsis is the major equatorial locus of high obliquity ice precipitation, the results indicate that the NSVs are the most favored location for ice streaming on high obliquity Mars. For the range of lithospheric heat flows calculated for the Hesperian and Amazonian, ice sheets are cold-based on the lobe tops and wet-based in the troughs. As only warm-based ice has significant erosive power, this supports the inference that ice streams shaped the NSVs.

[24] **Acknowledgments.** We are grateful to Michael Mischna for sharing his model output. We thank Michael Mischna, James Dohm, and two anonymous reviewers for comments and criticism. E. K. thanks Oded Aharonson, Bruce Murray, Dave Stevenson, Norbert Schorghofer, Andy Ingersoll and James Zimbelman for suggestions, and Sam Bowring for encouraging publication.

References

Carr, M. H., and J. W. Head III (2003), Oceans on Mars: An assessment of the observational evidence and possible fate, *J. Geophys. Res.*, *108*(E5), 5042, doi:10.1029/2002JE001963.

Dohm, J. M., R. C. Anderson, V. R. Baker, J. C. Ferris, T. M. Hare, R. G. Strom, L. P. Rudd, J. W. Rice Jr., R. R. Casavant, and D. H. Scott (2000), System of gigantic valleys northwest of Tharsis, Mars: Latent catastrophic flooding, northwest watershed, and implications for northern plains ocean, *Geophys. Res. Lett.*, *27*(21), 3559–3562, doi:10.1029/2000GL011728.

Dohm, J. M., et al. (2001), Latent outflow activity for western Tharsis, Mars: Significant flood record exposed, *J. Geophys. Res.*, *106*(E6), 12,301–12,314.

Fenton, M. M., B. T. Schreiner, E. Nielson, and J. G. Pawlowicz (1994), Quaternary geology, in *Geological Atlas of the Western Canada Sedimentary Basin*, edited by G. Mossop and I. Shetsen, pp. 413–420, Can. Soc. of Pet. Geol., Calgary, Alberta.

Forget, F., R. B. Haberle, B. Levrard, and J. W. Head (2006), Formation of glaciers on Mars by atmospheric precipitation at high obliquity, *Science*, *311*, 368–371.

Harrison, K. P., and R. E. Grimm (2004), Tharsis recharge: A source of groundwater for Martian outflow channels, *Geophys. Res. Lett.*, *31*, L14703, doi:10.1029/2004GL020502.

Head, J. W., and M. A. Kreslavsky (2001), Medusae Fossae Formation as volatile-rich sediments deposited at high obliquity: An hypothesis and tests, paper presented at the Conference on the Geophysical Detection of Subsurface Water on Mars, Lunar and Planet. Inst., Houston, Tex., 6–10 Aug.

Hindmarsh, R. C. A. (2001), Notes on basic glaciological computational methods and algorithms, in *Continuum Mechanics and Applications in Geophysics and the Environment*, edited by B. Straughan et al., pp. 222–249, Springer, Berlin.

Hudson, T. L., O. Aharonson, N. Schorghofer, C. B. Farmer, M. H. Hecht, and N. T. Bridges (2007), Water vapor diffusion in Mars subsurface environments, *J. Geophys. Res.*, *112*, E05016, doi:10.1029/2006JE002815.

Hynek, B. M., R. J. Phillips, and R. E. Arvidson (2003), Explosive volcanism in the Tharsis region: Global evidence in the Martian geologic record, *J. Geophys. Res.*, *108*(E9), 5111, doi:10.1029/2003JE002062.

Kreslavsky, M. A., and J. W. Head (2002), Fate of outflow channel effluents in the northern lowlands of Mars: The Vastitas Borealis Formation as a sublimation residue from frozen ponded bodies of water, *J. Geophys. Res.*, *107*(E12), 5121, doi:10.1029/2001JE001831.

Laskar, J., A. C. M. Correia, M. Gastineau, F. Joutel, B. Levrard, and P. Robutel (2004), Long term evolution and chaotic diffusion of the insolation quantities of Mars, *Icarus*, *170*(2), 343–364.

Le Meur, E., and P. Huybrechts (1996), A comparison of different ways of dealing with isostasy: Examples from modelling the Antarctic ice sheet during the last glacial cycle, *Ann. Glaciol.*, *23*, 309–317.

McGovern, P. J., S. C. Solomon, D. E. Smith, M. T. Zuber, M. Simons, M. A. Wieczorek, R. J. Phillips, G. A. Neumann, O. Aharonson, and J. W. Head (2004), Correction to "Localized gravity/topography admittance and correlation spectra on Mars: Implications for regional and global evolution," *J. Geophys. Res.*, *109*, E07007, doi:10.1029/2004JE002286.

McKenzie, D., J. Jackson, and K. Priestley (2005), Thermal structure of oceanic and continental lithosphere, *Earth Planet. Sci. Lett.*, *233*, 337–349.

McMenamin, D. S., and G. E. McGill (2006), Martian glacial melt and atmospheric methane, *Proc. Lunar Planet. Sci. Conf.*, *37th*, Abstract 1307.

Mischna, M. A. (2004), Origin and evolution of volatiles on Mars, Ph.D. thesis, Univ. of Calif., Los Angeles.

Mischna, M. A., and M. I. Richardson (2005), A reanalysis of water abundances in the Martian atmosphere at high obliquity, *Geophys. Res. Lett.*, *32*, L03201, doi:10.1029/2004GL021865.

Mischna, M. A., and M. I. Richardson (2006), Climate simulations of recent climate changes on Mars, paper presented at 2nd Mars Atmosphere Modelling and Observations Workshop, Eur. Space Agency, Granada, Spain, 27 Feb.–3 Mar.

Mischna, M. A., M. I. Richardson, R. J. Wilson, and D. J. McCleese (2003), On the orbital forcing of Martian water and CO_2 cycles: A general circulation model study with simplified volatile schemes, *J. Geophys. Res.*, *108*(E6), 5062, doi:10.1029/2003JE002051.

Parker, T. J. (1991), A comparison of the Martian Medusae Fossae Formation with terrestrial carbonate platforms, *Proc. Lunar Planet. Sci. Conf.*, *22nd*, 1029–1030.

Plaut, J. J., et al. (2007), Subsurface Radar Sounding of the South Polar Layered Deposits of Mars, *Science*, *316*, 92–95.

Rabassa, J., and C. M. Clapperton (1990), Quaternary glaciations of the southern Andes, *Quat. Sci. Rev.*, *9*, 153–174.

Rabassa, J., et al. (2000), Quaternary of Tierra del Fuego, southernmost South America: An updated review, *Quat. Int.*, *68–71*, 217–240.

Rabus, B., M. Eineder, A. Roth, and R. Bamler (2003), The shuttle radar topography mission: A new class of digital elevation models acquired by spaceborne radar, *ISPRS J. Photogramm. Remote Sens.*, *57*(4), 241–262.

Schultz, P. H., and A. B. Lutz (1988), Polar wandering of Mars, *Icarus*, *73*(1), 91–141.

Scott, D. H., and K. L. Tanaka (1982), Ignimbrites of Amazonis Planitia region of Mars, *J. Geophys. Res.*, *87*(B2), 1179–1190.

Scott, D. H., J. R. Zimbelman (1995), Geological map of Arsia Mons volcano, Mars, *U.S. Geol. Surv. Misc. Geol. Invest. Map*, *I-2480*.

Scott, E., and L. Wilson (2003), Did the Alba Patera and Syria Planum regions of Mars lose their lithospheric roots in convective overturn events?, *J. Geophys. Res.*, *108*(E5), 5035, doi:10.1029/2002JE001492.

Shean, D. E., J. W. Head III, J. L. Fastook, and D. R. Marchant (2007), Recent glaciation at high elevations on Arsia Mons, Mars: Implications for the formation and evolution of large tropical mountain glaciers, *J. Geophys. Res.*, *112*, E03004, doi:10.1029/2006JE002761.

Smith, D. E., et al. (2001), Mars Orbiter Laser Altimeter: Experiment summary after the first year of global mapping of Mars, *J. Geophys. Res.*, *106*(E10), 23,689–23,722, doi:10.1029/2000JE001364.

Tanaka, K. L. (2000), Dust and ice deposition in the Martian geological record, *Icarus*, *144*(2), 254–266.

Ward, A. W. (1979), Yardangs on Mars: Evidence of recent wind erosion, *J. Geophys. Res.*, *84*(B14), 8147–8166.

Zimbelman, J. R. (2006), Mapping of the Medusae Fossae Formation on Mars and the Northern Lowland plains of Venus, in *Abstracts of the Annual Meeting of Planetary Geological Mappers, Nampa, Idaho*, *U.S. Geol. Surv. Open File Rep.*, *2006–1263*.

Zurek, R. W., et al. (1992), Dynamics of the atmosphere of Mars, in *Mars*, edited by H. H. Kieffer et al., pp. 835–933, Univ. of Arizona Press, Tucson.

R. C. A. Hindmarsh, Physical Science Division, British Antarctic Survey, Natural Environment Research Council, High Cross, Cambridge CB3 0ET, UK. (rcah@bas.ac.uk)

E. S. Kite, Department of Earth and Planetary Science, University of California, Berkeley, 307 McCone Hall #4767, Berkeley, CA 94720-4767, USA. (kite@berkeley.edu)